Discrete TrkB-expressing neurons of the dorsomedial hypothalamus regulate feeding and thermogenesis

Jessica Houtz[a], Guey-Ying Liao[a], Juan Ji An[a], and Baoji Xu[a,1]

[a]Department of Neuroscience, The Scripps Research Institute, Jupiter, FL 33458

Edited by Richard D. Palmiter, University of Washington School of Medicine, Seattle, WA, and approved December 23, 2020 (received for review August 13, 2020)

Mutations in the TrkB neurotrophin receptor lead to profound obesity in humans, and expression of TrkB in the dorsomedial hypothalamus (DMH) is critical for maintaining energy homeostasis. However, the functional implications of TrkB-fexpressing neurons in the DMH (DMH^{TrkB}) on energy expenditure are unclear. Additionally, the neurocircuitry underlying the effect of DMH^{TrkB} neurons on energy homeostasis has not been explored. In this study, we show that activation of DMH^{TrkB} neurons leads to a robust increase in adaptive thermogenesis and energy expenditure without altering heart rate or blood pressure, while silencing DMH^{TrkB} neurons impairs thermogenesis. Furthermore, we reveal neuroanatomically and functionally distinct populations of DMH^{TrkB} neurons that regulate food intake or thermogenesis. Activation of DMH^{TrkB} neurons projecting to the raphe pallidus (RPa) stimulates thermogenesis and increased energy expenditure, whereas DMH^{TrkB} neurons that send collaterals to the paraventricular hypothalamus (PVH) and preoptic area (POA) inhibit feeding. Together, our findings provide evidence that DMH^{TrkB} neuronal activity plays an important role in regulating energy expenditure and delineate distinct neurocircuits that underly the separate effects of DMH^{TrkB} neuronal activity on food intake and thermogenesis.

TrkB | neurocircuitry | dorsomedial hypothalamus | energy expenditure | feeding

Impairments in energy homeostasis resulting from the compound effects of overeating and sedentary lifestyles have led to a profound increase in the rate of obesity around the world (1). Therapeutic strategies aimed at combating obesity by increasing energy expenditure or decreasing appetite have commonly failed due to counterregulatory mechanisms (2) and adverse side effects on cardiovascular physiology (3–5). To achieve safe and sustained weight loss, it will be essential to understand the mechanisms that govern and coordinate discrete physiological processes that contribute to energy homeostasis.

Adaptive thermogenesis is the process by which energy is converted into heat and occurs primarily in brown adipose tissue (BAT) in response to environmental cues (6). BAT has a particularly high capacity for dissipating energy from fat and thus represents an important component of energy homeostasis. The dorsomedial hypothalamus (DMH) in the brain is centrally positioned in an established thermoregulatory neurocircuit, receiving inputs from the preoptic area (POA) (7–9) and sending excitatory projections to preautonomic neurons in the raphe pallidus (RPa) (10–13) that promote sympathetic activity in BAT, leading to increased thermogenesis. Direct chemical stimulation of the DMH (14) or activation of select populations of thermogenic DMH neurons (9, 11, 12, 15) leads to increased body temperature and energy expenditure but also significantly increases heart rate and blood pressure (12, 13, 15, 16). An inability to target increased sympathetic tone specifically in BAT without affecting other target tissues has greatly hampered strategies to treat obesity by targeting thermogenesis (4, 5).

In addition to its influence on energy expenditure, the DMH also represents an important brain region in the regulation of feeding (17–19). Lesioning studies support an orexigenic role for the DMH (17), which can promote food intake through inhibitory projections to either the paraventricular hypothalamus (PVH) (18) or the arcuate nucleus (ARC) (20). Despite these early findings, evidence has also emerged that demonstrates the importance of anorexigenic populations of DMH neurons (19, 21, 22). We previously established that the activity of DMH neurons expressing the neurotrophin receptor TrkB (DMH^{TrkB}) is important for regulating feeding, showing that activation of DMH^{TrkB} neurons suppresses feeding and that deletion of the TrkB-encoding *Ntrk2* gene in the DMH results in hyperphagia and obesity (21). Furthermore, humans with mutations in the TrkB-encoding *NTRK2* gene exhibit severe obesity and impaired thermoregulation (23). However, it is unclear whether activation of DMH^{TrkB} neurons has a direct influence on adaptive thermogenesis. Additionally, the neurocircuitry through which DMH^{TrkB} neurons govern feeding or energy expenditure is unknown.

Here, we demonstrate that DMH^{TrkB} neuronal activity potently promotes energy expenditure by elevating thermogenesis and physical activity with a notable lack of influence on heart rate and blood pressure. We further reveal that DMH^{TrkB} neurons send diverging projections to the RPa or the POA and PVH to differentially regulate energy expenditure and food intake, respectively.

Results

DMH^{TrkB} Neurons Are Sensitive to Environmental Temperature. Since DMH neurons that respond to alterations in environmental temperature promote thermogenesis (9, 24), we first sought to

Significance

Neurons in the dorsomedial hypothalamus that express TrkB (DMH^{TrkB}) have been implicated in the regulation of appetite; however, their relevance to energy expenditure is less clear. This study reveals that activation of DMH^{TrkB} neurons potently induce thermogenesis and locomotor activity. Notably, increased energy expenditure mediated by DMH^{TrkB} neurons is not accompanied by increased heart rate or blood pressure, which have traditionally complicated weight loss therapies that target thermogenesis. Furthermore, our results reveal separate populations of DMH^{TrkB} neurons that form diverging neurocircuits to either the raphe pallidus or the paraventricular hypothalamus and preoptic area to independently regulate thermogenesis or feeding, respectively. These findings support a mechanism whereby DMH^{TrkB} neurons act through multiple pathways to promote weight loss without adverse cardiovascular consequences.

Author contributions: J.H., G.-Y.L., J.J.A., and B.X. designed research; J.H., G.-Y.L., and J.J.A. performed research; J.H. and G.-Y.L. analyzed data; and J.H. and B.X. wrote the paper.

The authors declare no competing interest.

This article is a PNAS Direct Submission.

[1]To whom correspondence may be addressed. Email: BXu@scripps.edu.

This article contains supporting information online at https://www.pnas.org/lookup/suppl/doi:10.1073/pnas.2017218118/-/DCSupplemental.

Published January 19, 2021.

determine whether DMH^{TrkB} neurons are temperature sensitive. We crossed *Ntrk2*$^{CreER/+}$ mice (25) with the Cre-dependent tdTomato reporter mouse line (Ai9) (26) to generate *Ntrk2*$^{CreER/+}$;Ai9 mice in which TrkB neurons are genetically labeled with tdTomato upon translocation of Cre-ERT2 protein to the nucleus induced by tamoxifen administration. Following the labeling of TrkB neurons with tamoxifen, *Ntrk2*$^{CreER/+}$;Ai9 mice were exposed to cold (10 °C) or warm (39 °C) temperatures, and immunostaining for Fos, a marker of activated neurons (27), was performed (Fig. 1 *A*–*C*). We found that exposure to cold activated 10.4 to 11.8% of TrkB-expressing neurons throughout the anterior to posterior extent of the DMH (Bregma −1.46 to −2.18 mm), while warmth only activated 7.7 to 8.6% of TrkB neurons, predominantly in the middle and posterior DMH (versus 1.9 to 3.1% activated DMH^{TrkB} neurons under the 30 °C thermoneutral condition) (Fig. 1*D*). Our results suggest that DMH^{TrkB} neurons respond to both increased and decreased ambient temperatures; however, statistical analysis indicates that there is no significant interaction between temperature sensitivity and anatomical location (repeated measures [RM] two-way ANOVA: interaction $F_{(4,18)} = 1.58$ and $P = 0.2225$). Thus, cold- and warm-sensitive DMH^{TrkB} neurons may not represent discrete populations.

Chemogenetic Manipulation of DMH^{TrkB} Neurons Alters Thermogenesis and Physical Activity. The observed increase in Fos^{+} neurons in response variation in temperature is consistent with a potential function for DMH^{TrkB} neurons in regulating body temperature through thermogenesis. To test how DMH^{TrkB} neuronal activity influences thermogenesis, we selectively expressed designer receptors exclusively activated by designer drugs (DREADD) in DMH^{TrkB} neurons (28). We delivered the adeno-associated virus (AAV) expressing the excitatory DREADD, hM3Dq (AAV8-hSyn-DIO-hM3-mCherry), into the DMH of *Ntrk2*$^{CreER/+}$ mice to selectively activate DMH^{TrkB} neurons using the ligand clozapine *N*-oxide (CNO) (Fig. 2*A* and *SI Appendix*, Fig. S1*A*) (28). Mice expressing either control mCherry or hM3 in DMH^{TrkB} neurons (DMH^{TrkB}:mCherry or DMH^{TrkB}:hM3 mice) were first acclimated to thermoneutrality (30 °C) prior to measuring the effects of CNO administration on body temperature and energy expenditure in order to mitigate the influence of basal thermogenesis

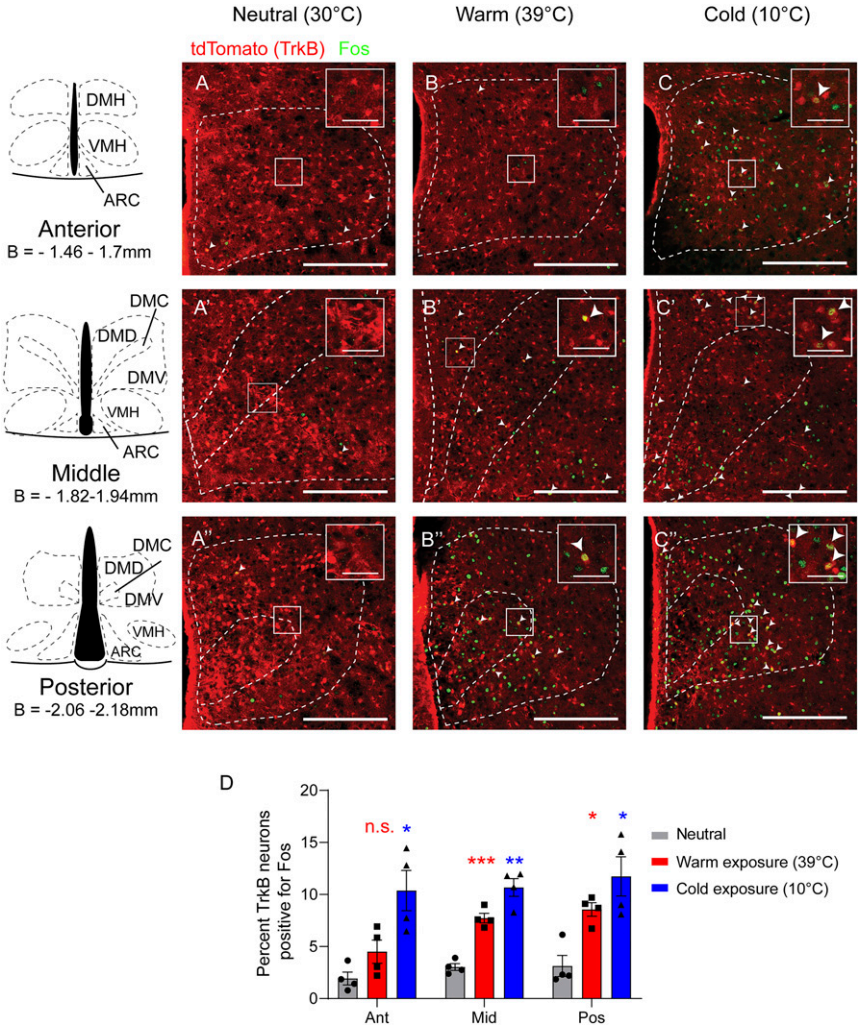

Fig. 1. DMH^{TrkB} neurons are sensitive to changes in environmental temperature. Representative images of Fos staining (green) in the DMH of *Ntrk2*$^{CreER/+}$;Ai9 reporter mice after exposure for 2 h to (*A*–*A″*) thermoneutral (30 °C), (*B*–*B″*) warm (39 °C), or (*C*–*C″*) cold (10 °C) temperatures. tdTomato (red) marks TrkB-expressing cells in reporter mice. (Scale bars, 250 μm; inset scale bars, 50 μm.) (*D*) Quantification of Fos induction in TrkB-expressing neurons in the anterior (Ant), middle (Mid), and posterior (Pos) DMH after mice were exposed to different temperatures. Two-way ANOVA: temperature, $F_{(2, 9)} = 18.68$; $P = 0.0006$; $n = 4$ mice per condition; Dunnett's posttest versus neutral; n.s. = not significant, $^{*}P < 0.05$, $^{**}P < 0.01$, and $^{***}P < 0.001$. Values represent mean ± SEM. DMH, dorsomedial hypothalamus; DMD, DMH dorsal division; DMC, DMH central division; DMV, DMH ventral division; VMH, ventromedial hypothalamus; ARC, arcuate nucleus; B, bregma.

that occurs under normal housing temperatures (22 °C) (29). Stimulation of DMH^{TrkB}:hM3 mice with CNO resulted in an acute and robust increase in body temperature compared with either vehicle (Veh) stimulation in the same mice or CNO treatment in DMH^{TrkB}:mCherry mice (Fig. 2 *B* and *C*).

Activation of thermogenesis in BAT represents the predominant mechanism for increasing body temperature in small mammals such as mice (29, 30). We asked whether the increase in core body temperature mediated by DMH^{TrkB} neurons was due to activation of BAT. Due to the proximity of BAT to the surface of the skin, thermal imaging has emerged as a useful tool for evaluating thermogenesis (30). Therefore, we employed infrared thermography to further investigate the effect of stimulating DMH^{TrkB} neurons on promoting thermogenesis locally in BAT (Fig. 2*D*). Following chemogenetic activation of DMH^{TrkB} neurons, we observed an increase in the subcutaneous temperature of the region above interscapular BAT (iBAT; Fig. 2*E*). Furthermore, we found an increase in the transcript level of the thermogenic marker, UCP-1, in iBAT 2 h after CNO stimulation in mice expressing hM3Dq in DMH^{TrkB} neurons but not mCherry (Fig. 2*F*). Thermogenic activity in BAT requires lipolysis, which is mediated in part by phosphorylation of hormone-sensitive lipase (HSL) to produce free fatty acids and glycerol (6). We observed that administration of CNO in mice expressing hM3, but not mCherry, in DMH^{TrkB} neurons led to an increase in both levels of p-HSL (*SI Appendix*, Fig. S1*B*) and glycerol (*SI Appendix*, Fig. S1*C*) in iBAT.

Thermogenesis is a metabolically demanding process that demands significant energy expenditure. Consistent with this requirement, we also found that chemogenetic activation of DMH^{TrkB} neurons drove a strong increase in energy expenditure (Fig. 2 *G* and *H*) while reducing respiratory exchange ratio (RER) (VCO_2/VO_2) (Fig. 2 *I* and *J*). A reduction in RER is indicative of a switch to preferential utilization of fat as a metabolic substrate.

In contrast to the reduction in RER that was observed after CNO treatment in DMH^{TrkB}:hM3 mice, CNO treatment increased RER in control DMH^{TrkB}:mCherry mice (Fig. 2 *I* and *J*). This nonspecific effect can likely be attributed to the conversion of CNO to clozapine in vivo (31). Clozapine is an atypical antipsychotic that has been documented as inhibiting lipolysis (32) and impairing thermogenesis (33). We found a significant interaction between the expression of DREADD virus and treatment with CNO (two-way RM ANOVA: interaction $F_{(1,16)} = 20.88$; $P = 0.0003$), indicating that DMH^{TrkB} neurons expressing hM3 with CNO can overcome the endogenous repressive effects of clozapine and further decrease RER beyond baseline levels. Together, our data indicate that DMH^{TrkB} neurons promote lipolysis in BAT to fuel thermogenesis, which results in increased energy expenditure and a lower RER. An additional effect of DMH^{TrkB} activation was a robust increase in locomotor activity, which could also contribute to the observed increase in total energy expenditure (Fig. 2 *K* and *L*).

Neurons in the DMH that stimulate thermogenesis through an increase in sympathetic nerve activity (SNA) also elicit increases in heart rate and blood pressure (12, 15, 16). Additionally, activation of SNA by cold or stress has been shown to promote subcutaneous vasoconstriction, resulting in a decrease in tail temperature in mice (8, 30, 34). Intriguingly, we found that stimulation of DMH^{TrkB} neurons in mice did not alter heart rate (Fig. 2*M*) or mean arterial pressure (Fig. 2*N*). Additionally, we did not observe a change in tail temperature upon activation of DMH^{TrkB} neurons (*SI Appendix*, Fig. S1*D*). These data support a mechanism through which DMH^{TkrB} neurons elevate energy expenditure and body temperature by selectively activating thermogenesis in BAT.

Next, we tested the necessity of DMH^{TrkB} neuronal activity for adaptive thermogenesis induced by cold exposure. We inactivated DMH^{TrkB} neurons by treating mice expressing the inhibitory chemogenetic receptor, hM4Di, in DMH^{TrkB} neurons (Fig. 3*A*) with CNO. Silencing DMH^{TrkB} neurons in cold-housed (10 °C) mice led to a reduction in body temperature (Fig. 3 *B* and *C*). We also observed a small decrease in energy expenditure in mice expressing hM4 in DMH^{TrkB} neurons following treatment with CNO compared to vehicle (two-way RM ANOVA: Veh versus CNO, $F_{(1, 11)} = 8.574$, and $P = 0.0137$); however, this effect was not significant when compared to oxygen consumption in control CNO-treated mice expressing mCherry in DMH^{TrkB} neurons (two-way RM ANOVA: mCherry versus hM4, $F_{(1, 11)} = 0.1502$, and $P = 0.7058$) (Fig. 3*E*). We also observed a significant increase in RER (Fig. 3 *F* and *G*), which could be attributed either to an increase in feeding that results from silencing DMH^{TrkB} neurons during the day (21) or inhibition of lipolysis that might be expected to occur concomitantly with the inhibition of BAT activity. Together, these findings support a necessary role for DMH^{TrkB} neuron activity in the maintenance of body temperature in response to cold exposure.

Separate populations of sympathetic neurons have been shown to innervate either white adipose tissue or BAT, indicating selectivity in sympathetic output at the level of the peripheral nervous system; however, the mechanisms governing this selectivity have not been defined (35). Since activation of DMH^{TrkB} neurons can induce thermogenesis without affecting heart rate, we hypothesized that these neurons may form a selective neurocircuit with sympathetic nerves that innervate BAT, but not the heart. To test this possibility, we performed polysynaptic anterograde tracing in DMH^{TrkB} neurons using Cre-dependent HSV129ΔTK-tdTomato (*SI Appendix*, Fig. S1*E*). Four days after infection, we observed connections between DMH^{TrkB} neurons and iBAT as evident by dense tdTomato labeling in UCP-1 expressing iBAT (*SI Appendix*, Fig. S1*F*). In contrast, we did not see tdTomato labeling in the heart or the sympathetic fibers innervating the heart (*SI Appendix*, Fig. S1*G*). Our findings suggest that DMH^{TrkB} neurons form selective neurocircuits with sympathetic neurons that innervate BAT tissue.

A DMH^{TrkB} → RPa Neurocircuit Regulates Thermogenesis and Energy Expenditure. Activation of DMH^{TrkB} neurons promotes negative energy balance by both inhibiting feeding (21) and increasing energy expenditure (Fig. 2). We performed anterograde tracing of DMH^{TrkB} neurons using AAV expressing Cre-dependent tdTomato (AAV2-CAG-FLEX-tdTomato) to determine the efferent targets responsible for mediating DMH^{TrkB} neuron functions (Fig. 4*A*). Following viral delivery to the DMH of $Ntrk2^{CreER/+}$ mice and induction with tamoxifen, DMH^{TrkB} neurons at the injection site were labeled with tdTomato (Fig. 4*B*), and their projections were observed in multiple brain regions, including the POA (Fig. 4*C*), PVH (Fig. 4*D*), ventrolateral periaqueductal gray matter (vlPAG) (Fig. 4*E*), and RPa (Fig. 4*F*). We also observed projections to the bed nucleus of the stria terminalis (BNST), anterior hypothalamus (AH), and ARC. Together, these data indicate that DMH^{TrkB} neurons have a broad projection field which may underly their functional diversity.

Sympathetic premotor neurons in the RPa are an established target of DMH neurons that activate thermogenesis (12, 13, 36). Since we observed that DMH^{TrkB} neurons send projections to the RPa, we first reasoned that a DMH^{TrkB} → RPa neurocircuit might be important for regulating thermogenesis and energy expenditure. To test this possibility, we developed a viral strategy to express the excitatory DREADD, hM3, in DMH^{TrkB} neurons in a projection specific manner. We simultaneously delivered retrograde AAV expressing Cre-dependent codon-optimized flippase (FLPo) (AAV2-retro-Ef1a-DIO-FLPo) to the RPa and AAV expressing FLPo-dependent hM3-mCherry or control mCherry (AAV2-Ef1a-fDIO-hM3-mCherry or AAV2-Ef1a-fDIO-mCherry) to the DMH in $Ntrk2^{CreER/+}$ mice (Fig. 4*G*). TrkB-expressing neurons in the DMH that project to the RPa ($DMH^{TrkB→RPa}$

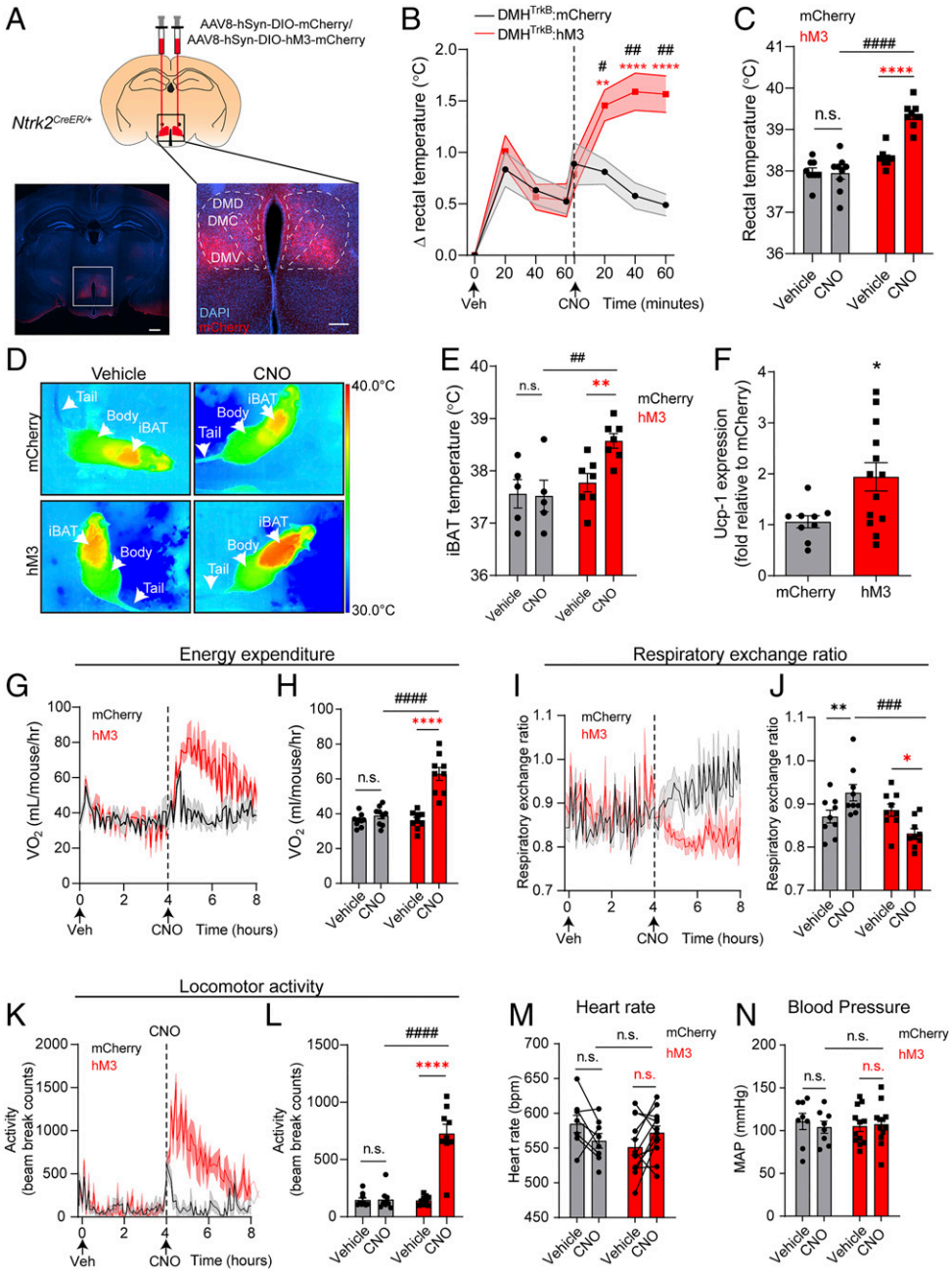

Fig. 2. DMH^{TrkB} neuronal activity drives negative energy balance. (*A*) Schematic of bilateral stereotactic delivery of AAV expressing Cre-dependent hM3-mCherry (AAV8-hSyn-DIO-hM3-mCherry) or mCherry (AAV8-hSyn-DIO-mCherry) into the DMH of *Ntrk2*$^{CreER/+}$ mice. Low-magnification scale bar, 500 μm; high-magnification scale bar, 200 μm. Mice housed at thermoneutrality expressing either mCherry (gray, $n = 9$) or hM3-mCherry (red, $n = 9$) in DMH^{TrkB} neurons were treated with Veh or CNO during the light cycle. (*B*) Rectal temperature. Two-way RM ANOVA: mCherry versus hM3, $F_{(1,\ 16)} = 10.11$, and $P = 0.0058$. (*C*) Average rectal temperatures 60 min after treatment. Two-way RM ANOVA: mCherry versus hM3, $F_{(1,\ 16)} = 36.55$, and $P < 0.0001$. (*D*) Representative thermal images. (*E*) iBAT temperature of mice housed at thermoneutrality expressing mCherry ($n = 5$) or hM3 ($n = 7$) in DMH^{TrkB} neurons 60 min postinjection with either vehicle or CNO. Two-way RM ANOVA: mCherry versus hM3, $F_{(1,\ 10)} = 6.350$, and $P = 0.0304$. (*F*) Levels of *Ucp1* mRNA in iBAT from mice expressing hM3 or mCherry in DMH^{TrkB} neurons 2 h following treatment with CNO (n= 9 mCherry and n= 13 hM3; unpaired, two-tailed t test, and $P = 0.0207$). (*G*) Oxygen consumption (VO_2) over 4 h after treatment with Veh (0 to 4 h) and CNO (4 to 8 h). Mixed-effects model: mCherry versus hM3 (post-CNO), $F_{(1,\ 16)} = 26.89$, and $P < 0.0001$. (*H*) VO_2 for the duration of the first 4 h after treatment. Two-way RM ANOVA: mCherry versus hM3, $F_{(1,\ 16)} = 17.64$, and $P = 0.0007$. (*I*) RER over 4 h following treatment. Mixed-effects model: mCherry versus hM3 expression (post-CNO), $F_{(1,\ 16)} = 16.65$, and $P = 0.0009$. (*J*) Average RER for the duration of the first 4 h after treatment. Two-way RM ANOVA: mCherry versus hM3 expression, $F_{(1,\ 16)} = 5.072$, and $P = 0.0387$. (*K*) Locomotor activity over 4 h after treatment. Mixed-effects model: mCherry versus hM3 (post-CNO), $F_{(1,\ 16)} = 39.78$, and $P < 0.0001$. (*L*) Average locomotor activity for the duration of the first 4 h after treatment. Two-way RM ANOVA: mCherry versus hM3, $F_{(1,\ 16)} = 30.86$, and $P < 0.0001$. (*M* and *N*) Heart rate and mean arterial pressure (MAP) in mice expressing mCherry or hM3 in DMH^{TrkB} neurons 1 h after vehicle or CNO treatment. Two-way RM ANOVA for heart rate: mCherry versus hM3 expression, $F_{(1,\ 18)} = 0.6447$, and $P = 0.4325$. Two-way RM ANOVA for MAP: mCherry versus hM3 expression, $F_{(1,\ 18)} = 0.\ 01210$, and $P = 0.9136$. $n = 8$ mCherry mice and 12 hM3 mice. Values represent mean ± SEM. (*B*, *C*, *E*, and *G*–*N*) Sidak posttest (red * for hM3-Veh versus hM3-CNO, black * for mCherry-Veh versus mCherry-CNO, and # for mCherry versus hM3 post-CNO: n.s. = not significant; * and #, $P < 0.05$; ** and ##, $P < 0.01$; *** and ###, $P < 0.001$; **** and ####, $P < 0.0001$).

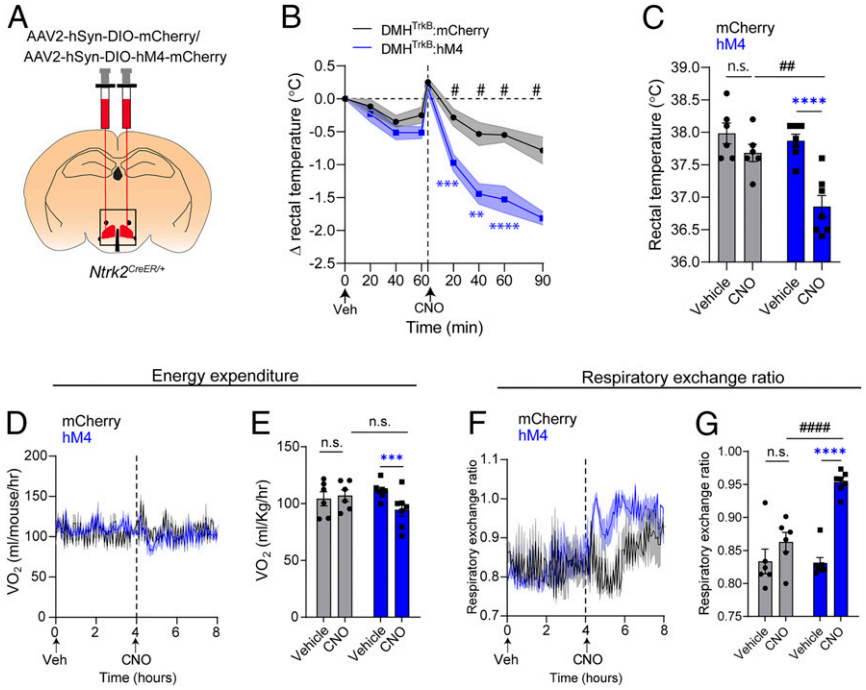

Fig. 3. DMH^{TrkB} neurons are necessary for cold-induced thermogenesis. (*A*) Schematic of bilateral stereotactic delivery of AAV expressing Cre-dependent inhibitory hM4-mCherry (AAV2-hSyn-DIO-hM4-mCherry) or mCherry (AAV2-hSyn-DIO-mCherry) into the DMH of $Ntrk2^{CreER/+}$. (*B–G*) Mice housed at 10 °C expressing either mCherry (gray, $n = 6$) or hM4-mCherry (blue, $n = 7$) in DMH^{TrkB} neurons were treated with vehicle (Veh) or CNO during the light cycle. (*B*) Rectal temperature of mice following treatment with Veh (0 to 60 min) or CNO (0 to 90 min). Two-way RM ANOVA: mCherry versus hM4, $F_{(1,\ 11)} = 20.40$, and $P = 0.0009$. (*C*) Average rectal temperatures 60 min after treatment. Two-way RM ANOVA: mCherry versus hM4, $F_{(1,\ 11)} = 7.577$, and $P = 0.0188$. (*D*) Oxygen consumption over 4 h after treatment. Mixed-effects model: mCherry versus hM4 expression (post-CNO), $F_{(1,\ 11)} = 3.066$, and $P = 0.1078$. (*E*) Average VO_2 for the duration of the first 4 h after treatment. Two-way RM ANOVA: mCherry versus hM4 expression, $F_{(1,\ 11)} = 0.1502$, and $P = 0.7058$). (*F*) RER over 4 h after treatment. Mixed-effects model: mCherry versus hM4 (post-CNO), $F_{(1,\ 11)} = 39.28$, and $P < 0.0001$. (*G*) RER for the duration of the first 4 h after treatment. Two-way RM ANOVA: mCherry versus hM4, $F_{(1,\ 11)} = 8.633$, and $P = 0.0135$. Values represent mean ± SEM (*B–G*). Sidak posttest (blue * for hM4-Veh versus hM4-CNO, black * for mCherry-Veh versus mCherry-CNO, and # for mCherry versus hM4 post-CNO: n.s. = not significant; $^{\#}P < 0.05$; ** and $^{\#\#}$, $P < 0.01$; ***$P < 0.001$; **** and $^{\#\#\#\#}$, $P < 0.0001$).

neurons) become infected with AAV2-retro-Ef1a-DIO-FLPo, and Cre expressed in TrkB neurons in $Ntrk2^{CreER/+}$ mice can induce expression of FLP recombinase, allowing for subsequent expression of hM3-mCherry or mCherry.

We confirmed expression of mCherry in neurons in the DMH (Fig. 4*H*) and in axon terminals in the RPa (Fig. 4*I*). When AAV2-Ef1a-fDIO-mCherry/hM3-mCherry were injected into the DMH simultaneously with AAV2-retro-Ef1a-DIO-FLPo into the RPa of wild-type mice that lack Cre expression in TrkB-expressing neurons, we saw no mCherry signal (*SI Appendix*, Fig. S2 *A–C*). Additionally, injection of AAV2-Ef1a-fDIO-mCherry/hM3-mCherry alone into the DMH of $Ntrk2^{CreER/+}$ mice without a second injection of AAV2-retro-Ef1a-DIO-FLPo into the RPa was insufficient to induce expression of mCherry (*SI Appendix*, Fig. S2 *D–F*). Treatment with CNO did not result in increased Fos expression in $DMH^{TrkB\rightarrow RPa}$ neurons expressing mCherry compared with hM3 (*SI Appendix*, Fig. S2 *G* and *H*). These results support our ability to target specific DMH^{TrkB} neurons for chemogenetic activation based on their projection target.

We then tested the effect of activating the DMH^{TrkB} → RPa neurocircuit on thermogenesis and energy expenditure. Treatment with CNO, but not vehicle, increased iBAT temperature (Fig. 4*J*) and expression of *Ucp1* (Fig. 4*K*) in $Ntrk2^{CreER/+}$ mice expressing hM3 in $DMH^{TrkB\rightarrow RPa}$ neurons compared with mCherry expressing control mice. Treatment of control mCherry mice with CNO led to a decrease in iBAT temperature, which we hypothesize is attributed to the nonspecific antithermogenic effect of clozapine. Consistent with the activation of thermogenesis that was observed upon stimulation of $DMH^{TrkB\rightarrow RPa}$ neurons, we saw a trend toward increased oxygen consumption in mice treated with CNO and expressing hM3 compared with mice expressing mCherry in $DMH^{TrkB\rightarrow RPa}$ neurons ($P = 0.0584$) (Fig. 4*L*). Furthermore, treatment with CNO resulted in an increase in oxygen consumption compared with vehicle treatment in mice expressing hM3 in $DMH^{TrkB\rightarrow RPa}$ neurons (Fig. 4*M*). In contrast to the effect of activating all DMH^{TrkB} neurons, stimulation of $DMH^{TrkB\rightarrow RPa}$ neurons did not alter RER (Fig. 4 *N* and *O*) or physical activity (*SI Appendix*, Fig. S3 *A* and *B*). We previously showed that activation of DMH^{TrkB} neurons suppresses nocturnal feeding (21); however, stimulation of a DMH^{TrkB} → RPa circuit had no effect on food intake (Fig. 4*P*). Although activation of $DMH^{TrkB\rightarrow RPa}$ neurons increased thermogenesis in BAT to a similar level as previously observed, the DMH^{TrkB} → RPa neurocircuit was not sufficient to drive total energy expenditure to the same extent or duration as that observed for activation of all DMH^{TrkB} neurons (Figs. 2*G* and 4*L*). Nevertheless, DMH^{TrkB} → RPa neurons contribute to the net negative effect of activating DMH^{TrkB} neurons on energy balance without contributing to alterations in fat metabolism or feeding.

Glutamatergic neurons in the anterior and dorsal compartments of the DMH that express bombesin receptor subtype 3 (*Brs3*) or the leptin receptor (*Lepr*) have been shown to project to the RPa and promote thermogenesis (15, 24, 37). We previously showed that there is very little overlap between *Lepr* and TrkB expression in the DMH (21), and, in contrast to DMH^{TrkB} neurons that do not affect cardiovascular function, both DMH^{Brs3} and DMH^{LepR} neurons influence heart rate in addition to body temperature (15, 16). To determine whether there is any overlap between RPa-projecting DMH^{TrkB} and DMH^{Brs3} neurons,

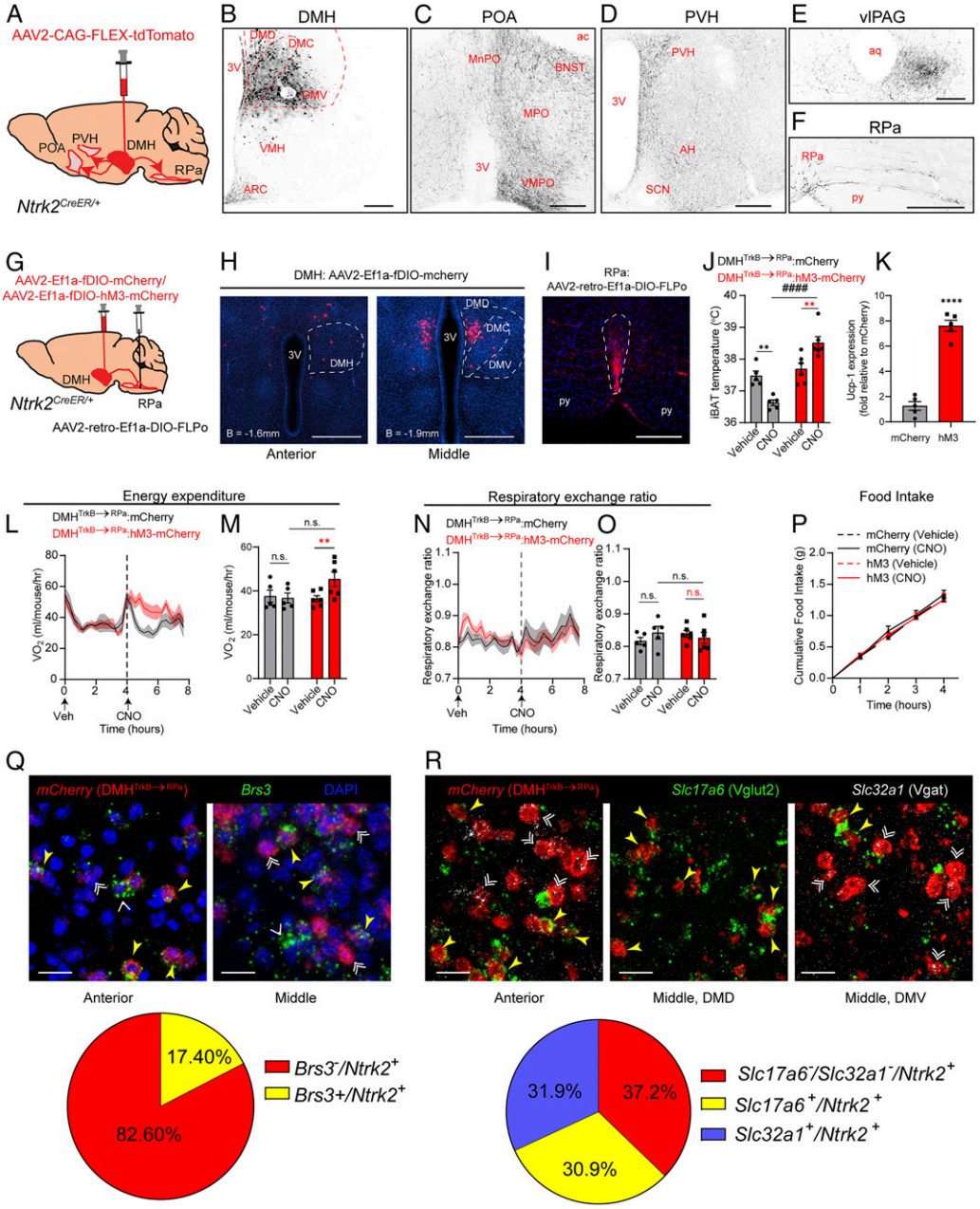

Fig. 4. A DMH^{TrkB} → RPa neurocircuit regulates energy expenditure and body temperature. (*A*) Diagram of anterograde tracing of DMH^{TrkB} neurons in *Ntrk2*$^{CreER/+}$ mice unilaterally injected with AAV2-CAG-FLEX-TdTomato. (*B*) Injection site. (*C*–*F*) Projection targets: (*C*) POA including the median preoptic area, MPO, and VMPO and the BNST; (*D*) PVH and AH; (*E*) vlPAG; and (*F*) RPa. (Scale bars, 200 μm.) (*G*) Schematic of stereotactic delivery of retrograde AAV expressing Cre-dependent FLPo (AAV2-retro-Ef1a-DIO-FLPo) and AAV2-CMV-GFP to the RPa, and FLP-dependent (fDIO) mCherry or hM3-mCherry expressing virus to the DMH in *Ntrk2*$^{CreER/+}$ mice. (*H*) Expression of mCherry (red) in DMH$^{TrkB→RPa}$ neurons. (Scale bar, 500 μm.) (*I*) mCherry-labeled DMH$^{TrkB→RPa}$ terminals are detected in the RPa (outlined). (Scale bar, 200 μm.) (*J*–*O*) Mice housed at thermoneutrality and expressing hM3-mCherry (red, $n = 6$) or mCherry (gray, $n = 5$) in DMH$^{TrkB→RPa}$ neurons were treated with Veh or CNO during the light cycle. (*J*) BAT temperature 60 min after Veh or CNO treatment. Two-way RM ANOVA: mCherry versus hM3, $F_{(1, 9)} = 29.24$, and $P = 0.0004$. (*K*) Relative levels of *Ucp1* mRNA in BAT 2 h post-CNO treatment. Unpaired, two-tailed *t* test, $P < 0.0001$. (*L*) Oxygen consumption after treatment. Two-way RM ANOVA: mCherry versus hM3 (post-CNO), $F_{(1, 9)} = 4.695$, and $P = 0.0584$. (*M*) Average oxygen consumption for the duration of the first 4 h after treatment. Two-way RM ANOVA: mCherry versus hM3, $F_{(1, 9)} = 1.227$, and $P = 0.2967$. (*N*) RER after treatment with vehicle or CNO. Two-way RM ANOVA: mCherry versus hM3 (post-CNO), $F_{(1, 9)} = 0.2985$, and $P = 0.5985$. (*O*) Average RER for the duration of the first 4 h after treatment. Two-way RM ANOVA: mCherry versus hM3, $F_{(1, 9)} = 0.03257$, and $P = 0.8608$. (*P*) Nocturnal food intake of mice expressing mCherry or hM3 in DMH$^{TrkB→RPa}$ neurons after treatment with vehicle or CNO. Two-way RM ANOVA: mCherry versus hM3, $F_{(1, 16)} = 0.02664$, and $P = 0.8724$. (*Q*) Detection of *Brs3* (green) and mCherry (red) expression by ISH in the anterior (*Left*) and middle (*Right*) DMH of DMH$^{TrkB→RPa}$:mCherry expressing mice. Yellow arrowheads indicate *Brs3*$^{+}$ DMH$^{TrkB→RPa}$ neurons. White double arrowheads indicate *Brs3*$^{-}$ DMH$^{TrkB→RPa}$ neurons. Single white arrowheads indicate *Brs3*$^{+}$ *mCherry*$^{-}$. (Scale bars, 20 μm.) (*R*) In situ detection of *Slc17a6* (Vglut2, green) and *Slc32a1* (Vgat, white) in the anterior and middle-dorsal and middle-ventral DMH of DMH$^{TrkB→RPa}$:mCherry mice. Yellow arrowheads indicate *Vglut*$^{+}$ DMH$^{TrkB→RPa}$ neurons. Double white arrowheads indicate *Vgat*$^{+}$ DMH$^{TrkB→RPa}$ neurons. (Scale bars, 20 μm.) (*Q* and *R*) Representative images are from $n = 3$ animals. Values represent mean ± SEM. Sidak posttest (red * for hM3-Veh versus hM3-CNO, black * for mCherry-Veh versus mCherry-CNO, and # for mCherry versus hM3 post CNO; n.s. = not significant; $^{**}P < 0.01$; **** and ####, $P < 0.0001$). 3V, third ventricle; ac, anterior commissure; py, pyramid; SCN, suprachiasmatic nucleus.

we performed fluorescent in situ hybridization (ISH) for *Brs3* and *mCherry* expression in the DMH of $DMH^{TrkB\rightarrow RPa}$:mCherry mice (Fig. 4*Q*). Although we observed partial overlap between *mCherry* (representing $DMH^{TrkB\rightarrow RPa}$ neurons) and *Brs3* expression, not all *Brs3*-expressing neurons expressed *mCherry*. Conversely, we observed many *mCherry*-positive, *Brs3*-negative neurons, indicating that DMH^{Brs3} and $DMH^{TrkB\rightarrow RPa}$ neurons are not identical populations. We also analyzed the expression of *Slc17a6* (Vglut2) and *Slc32a1* (Vgat) in $DMH^{TrkB\rightarrow RPa}$ neurons, which are markers of excitatory and inhibitory neurotransmission, respectively (Fig. 4*R*). Other DMH → RPa neurons have been characterized as predominantly glutamatergic (Vglut2 expressing) (12). Surprisingly, we found that $DMH^{TrkB\rightarrow RPa}$ neurons are a heterogeneous population consisting of both Vglut2- and Vgat-expressing neurons, as well as some neurons that do not appear to express either neurotransmitter at levels detectable by ISH.

DMH^{TrkB} Neurons Collateralize to the PVH and POA to Regulate Feeding and Metabolism. Activation of DMH^{TrkB} neurons drives high levels of oxygen consumption concurrent with stimulation of lipolysis (Fig. 2 and *SI Appendix*, Fig. S1) and inhibition of homeostatic feeding (21). Since $DMH^{TrkB\rightarrow RPa}$ neurons do not influence RER or feeding, we aimed to determine the identity of a DMH^{TrkB} neurocircuit that regulates these other components of energy balance. Neurons in the PVH that express brain-derived neurotrophic factor (BDNF—a high-affinity TrkB ligand) have been implicated in regulating food intake, energy expenditure, and locomotor activity; however, the identity of their presynaptic partners is unknown (38). Our anterograde tracing results indicate that the PVH receives projections from DMH^{TrkB} neurons (Fig. 4*D*); thus, we hypothesized that a DMH^{TrkB}→PVH pathway might account for the effect of DMH^{TrkB} neuronal activity on feeding. Using the same projection-specific viral strategy described earlier, we expressed mCherry or hM3-mCherry in PVH-projecting DMH^{TrkB} neurons (Fig. 5*A*). $DMH^{TrkB\rightarrow PVH}$:mCherry neurons are mainly present in the middle-to-posterior ventral DMH (DMV) and the medial-ventral part of the central DMH (DMC) (Fig. 5*B*). We confirmed proper targeting of the PVH by coinjection of AAV-GFP with AAV-retro-DIO-FLPo. PVH neurons at the injection site expressed GFP and received dense innervation by $mCherry^{+}$ $DMH^{TrkB\rightarrow PVH}$ fibers (Fig. 5 *C* and *C′*). These results indicate successful targeting of a DMH^{TrkB} → PVH neurocircuit for chemogenetic manipulation.

Activation of $DMH^{TrkB\rightarrow PVH}$ neurons increased iBAT temperature 1 h after treatment with CNO (Fig. 5*D*); however, only a small increase in energy expenditure, mainly restricted to the first hour, was evident (Fig. 5 *E* and *F*). Similar to $DMH^{TrkB\rightarrow RPa}$ neurons, the DMH^{TrkB} → PVH neurocircuit was not sufficient to drive oxygen consumption to the same extent as activation of all DMH^{TrkB} neurons, nor did it have any influence on physical activity (*SI Appendix*, Fig. S3 *C* and *D*). Stimulation of the DMH^{TrkB} → PVH circuit lowers RER despite the nonspecific effect of CNO which increases RER in control $DMH^{TrkB\rightarrow PVH}$:mCherry animals (Fig. 5 *G* and *H*) and inhibits nocturnal feeding in mice (Fig. 5*I*). Thus, $DMH^{TrkB\rightarrow PVH}$ neurons contribute to negative energy balance predominantly by regulating nutrient consumption and fatty acid utilization, but not thermogenesis.

Analysis of *Slc17a6* (Vglut2) and *Slc32a1* (Vgat) expression in $DMH^{TrkB\rightarrow PVH}$ neurons labeled with mCherry revealed a slight bias in the number of inhibitory Vgat-expressing $DMH^{TrkB\rightarrow PVH}$ neurons (40%) over those that express Vglut2 (24.6%) (*SI Appendix*, Fig. S5 *A–D*). However, similar to $DMH^{TrkB\rightarrow RPa}$ neurons, we found many $DMH^{TrkB\rightarrow PVH}$ neurons that did not appear to express either Vglut2 or Vgat (*SI Appendix*, Fig. S5 *A–D*).

BDNF-expressing neurons that project to the DMH are also located in the POA (POA^{BDNF}) (8). However, as POA^{BDNF} neurons negatively regulate body temperature by inhibiting BAT activity, DMH^{TrkB} neurons projecting to the POA could contribute to increased energy expenditure by inhibiting POA^{BDNF} neurons. Thus, we targeted expression of mCherry or hM3-mCherry to $DMH^{TrkB\rightarrow POA}$ neurons (Fig. 5 *J* and *K*) to evaluate the function of a DMH^{TrkB} → POA neurocircuit on energy expenditure. Expression of GFP at the injection site was predominantly restricted to the ventromedial preoptic area (VMPO) (Fig. 5 *L* and *L′*, *i*), where warm-sensitive BDNF-expressing neurons have previously been reported (8). While $mCherry^{+}$ $DMH^{TrkB\rightarrow POA}$ axon terminals were evident in the VMPO (Fig. 5 *L* and *L′*, *ii*), we also noted collateralization to the medial preoptic area (MPO) as well as the anteroventral periventricular nucleus (Fig. 5*L*). These data indicate that $DMH^{TrkB\rightarrow POA}$ neurons have a large projection field within the POA, which is likely not restricted to POA^{BDNF} neurons. Activation of $DMH^{TrkB\rightarrow POA}$ neurons expressing hM3-mCherry with CNO had no significant effect on BAT temperature (Fig. 5*M*), oxygen consumption (Fig. 5 *N* and *O*), RER (Fig. 5 *P* and *Q*), or physical activity (*SI Appendix*, Fig. S3 *E* and *F*). However, we noted a slight trend toward a lower RER in the fourth hour following CNO treatment in mice expressing hM3-mCherry compared with mCherry (Fig. 5*P*). As was observed for the activation of the DMH^{TrkB} → PVH circuit, we saw that treatment with CNO inhibited nocturnal feeding in mice expressing hM3 compared with mCherry expression in $DMH^{TrkB\rightarrow POA}$ neurons or compared with vehicle treatment (Fig. 5*R*). Together, these results demonstrate that $DMH^{TrkB\rightarrow POA}$ and $DMH^{TrkB\rightarrow PVH}$ neurons have a redundant function in the regulation of food intake.

$DMH^{TrkB\rightarrow PVH}$ and $DMH^{TrkB\rightarrow POA}$ neurons also appeared to have a similar anatomical distribution within the DMH (Fig. 5 *B* and *K*). These results raise the possibility that a single population of DMH^{TrkB} neurons sends projections to both the PVH and the POA. Indeed, we observed that $DMH^{TrkB\rightarrow PVH}$ neurons send collaterals to the POA, including both the MPO and VMPO, and to the BNST (*SI Appendix*, Fig. S4 *A–C* and *C′*), but not the RPa (*SI Appendix*, Fig. S4*D*). Similarly, we observed $DMH^{TrkB\rightarrow POA}$ collaterals in the PVH (*SI Appendix*, Fig. S4 *E–G* and *G′*), but $DMH^{TrkB\rightarrow RPa}$ collaterals were not apparent in either the POA (*SI Appendix*, Fig. S4 *H–J*) or the PVH (*SI Appendix*, Fig. S4*K*).

To further confirm the overlap between $DMH^{TrkB\rightarrow PVH}$ and $DMH^{TrkB\rightarrow POA}$ populations, we simultaneously injected cholera toxin B subunit (CTB) labeled with two different fluorophores, Alexa Fluor 488 or 647 (CTB-488 or CTB-647), into the PVH and the POA of $Ntrk2^{CreER/+}$;Ai9/+ mice induced with tamoxifen (*SI Appendix*, Fig. S4 *L–N*). Neurons in the DMH that project to the PVH were evident by labeling with CTB-488, while those that project to the POA were labeled with CTB-647 (*SI Appendix*, Fig. S4*O*), and TrkB-expressing neurons were labeled with tdTomato (*SI Appendix*, Fig. S4*P*). PVH- and POA-projecting DMH neurons were concentrated in the ventral part of the middle-to-posterior DMH. Upon further inspection, we found that most DMH neurons that send collateral projections to both the POA and PVH express TrkB (*SI Appendix*, Fig. S4 *Q–T*, arrowheads), supporting the existence of a population of DMH^{TrkB} neurons that send projections to both the POA and the PVH.

Discussion

Expression of TrkB in the brain is essential for maintaining normal body weight in both humans and rodents (23, 39, 40). We have previously reported that TrkB-expressing neurons in the DMH (21) and the PVH (41) are essential for regulating food intake, and DMH^{TrkB} neuronal activity modulates homeostatic feeding. Although loss of TrkB signaling in the DMH also leads to reduced oxygen consumption and physical activity (21), these consequences could be secondary to excessive weight gain. In the present study, we establish that DMH^{TrkB} neuronal activity has a direct influence on energy expenditure and body temperature that does not extend to influence components of cardiovascular physiology, which are typically affected by other DMH neuron populations. Furthermore, we reveal diverging DMH^{TrkB} neurocircuits

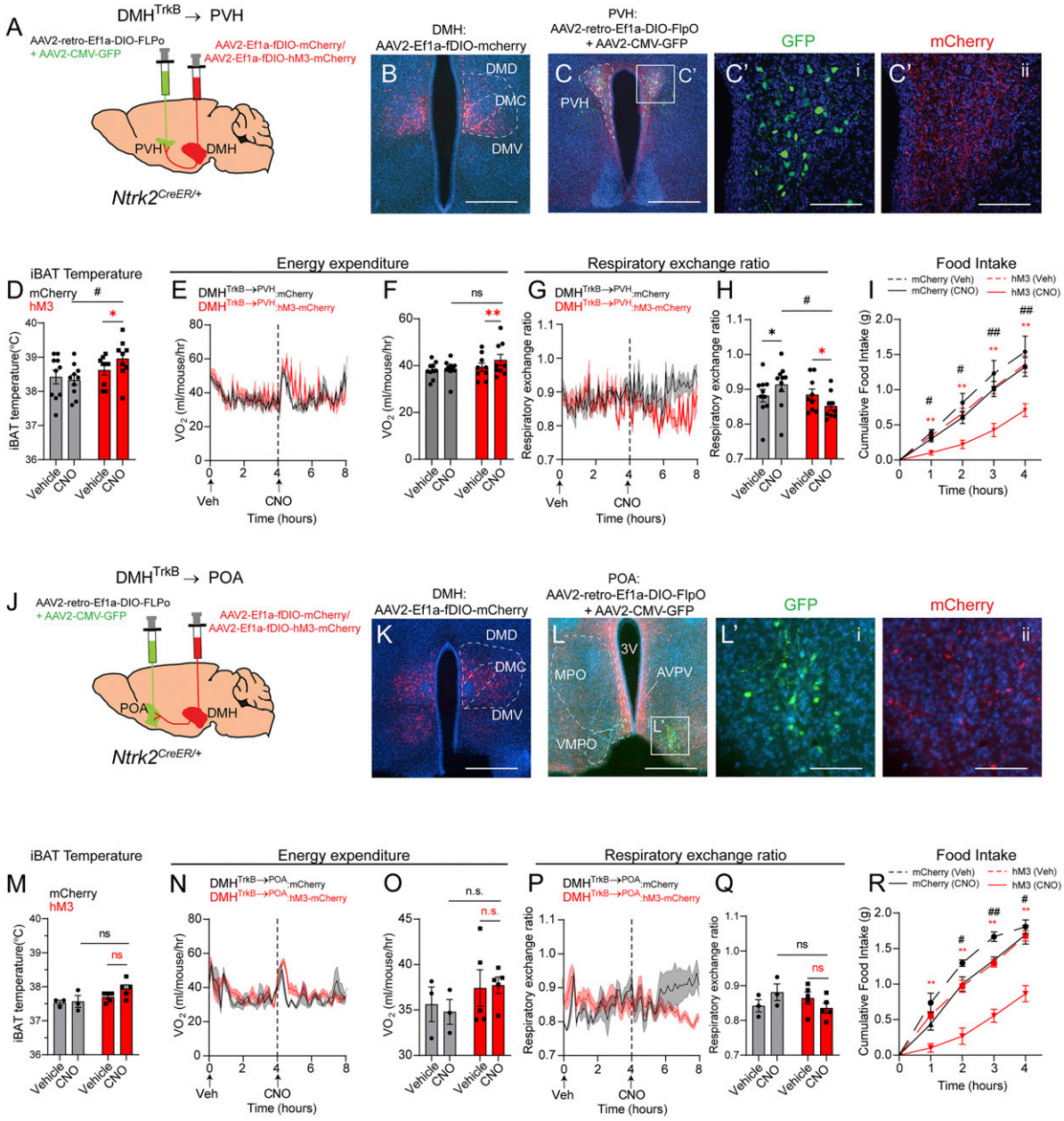

Fig. 5. DMH^{TrkB} neurons project to the PVH and POA to regulate feeding and metabolism. (*A*) Strategy for projection-specific targeting of mCherry or hM3-mCherry expression in DMH^{TrkB} neurons. Retrograde AAV expressing Cre-dependent FLPo (AAV2-retro-Ef1a-DIO-FLPo) and AAV-GFP are delivered to the PVH, while Flp-dependent mCherry or hM3-mCherry–expressing virus is injected into the DMH in *Ntrk2*$^{CreER/+}$ mice. (*B*) Expression of mCherry in DMH$^{TrkB\rightarrow PVH}$ neurons. (Scale bar, 500 μm.) (*C* and *C′*) Expression of GFP marking the injection site of retrograde AAV2-retro-Ef1a-DIO-FLPo in the PVH (*C′*, *i*) and mCherry in axonal terminals of DMH^{TrkB} neurons in the PVH (*C′*, *ii*). Scale bars, 500 μm in *B* and 100 μm in *C′*. (*D–H*) Mice housed at thermoneutrality and expressing mCherry (gray, $n = 10$) or hM3-mCherry (red, $n = 9$) in DMH$^{TrkB\rightarrow PVH}$ neurons were treated with Veh and then CNO during the light cycle. (*D*) iBAT temperature. Two-way RM ANOVA: mCherry versus hM3, $F_{(1,\ 17)} = 3.178$, and $P = 0.0925$. (*E*) Oxygen consumption. Mixed-effects model: mCherry versus hM3 (post-CNO), $F_{(1,\ 17)} = 0.4561$, and $P = 0.5085$. (*F*) Average oxygen consumption for the duration of 4 h following treatment. Two-way RM ANOVA: mCherry versus hM3, $F_{(1,\ 17)} = 1.252$, and $P = 0.2787$. (*G*) RER. Mixed-effects model: mCherry versus hM3 (post-CNO), $F_{(1,\ 17)} = 5.311$, and $P = 0.0341$. (*H*) Average RER for the duration of 4 h following treatment. Two-way RM ANOVA: mCherry versus hM3, $F_{(1,\ 17)} = 1.614$, and $P = 0.008168$. (*I*) Nocturnal food intake of mice expressing mCherry or hM3 in DMH$^{TrkB\rightarrow PVH}$ neurons postinjection of vehicle or CNO. Two-way RM ANOVA: mCherry versus hM3, $F_{(1,\ 17)} = 4.913$, and $P = 0.0406$. (*J*) Schematic for projection-specific targeting of DMH$^{TrkB\rightarrow POA}$ neurons. (*K*) Expression of mCherry in DMH$^{TrkB\rightarrow POA}$ neurons. (Scale bar, 500 μm.) (*L* and *L′*) Expression of GFP marking the injection site of AAV2-retro-Ef1a-DIO-FLPo in the POA and mCherry in axonal terminals of DMH^{TrkB} neurons in the POA. (Scale bars, 500 μm in *L* and 100 μm in *L′*. (*M–O*) Mice housed at thermoneutrality and expressing mCherry (gray, $n = 3$) or hM3-mCherry (red, $n = 5$) in DMH$^{TrkB\rightarrow POA}$ neurons were treated with Veh and then CNO during the light cycle. (*M*) iBAT temperature. Two-way RM ANOVA: mCherry versus hM3, $F_{(1,\ 6)} = 5.031$, and $P = 0.0661$. (*N*) Oxygen consumption. Two-way RM ANOVA: mCherry versus hM3 (post-CNO), $F_{(1,\ 6)} = 3.557$, and $P = 0.1083$. (*O*) Average oxygen consumption for the duration of 4 h following treatment. Two-way RM ANOVA: mCherry versus hM3, $F_{(1,\ 6)} = 1.475$, and $P = 0.2701$). (*P*) RER. Two-way RM ANOVA: mCherry versus hM3 (post-CNO), $F_{(1,\ 6)} = 2.985$, and $P = 0.1348$. (*Q*) Average respiratory ratio for the duration of 4 h following treatment. Two-way RM ANOVA; mCherry versus hM3, $F_{(1,\ 6)} = 0.2390$, and $P = 0.6423$. (*R*) Nocturnal food intake of mice expressing mCherry or hM3 in DMH$^{TrkB\rightarrow POA}$ neurons. Two-way RM ANOVA: mCherry versus hM3, $F_{(1,\ 6)} = 24.98$, and $P = 0.0025$. Values represent mean ± SEM. Sidak posttest (* for Veh versus CNO, $^{\#}$ for mCherry versus hM3; * and $^{\#}$, $P < 0.05$; ** and $^{\#\#}$, $P < 0.01$; n.s. = not significant).

are responsible for regulating adaptive thermogenesis, physical activity, fat metabolism, and appetite. Together, our findings support an integral role for DMH^{TrkB} neurons in coordinating multiple arms of energy balance and provide insight into the neural mechanisms underlying their functions, which may be expected to inform efforts to target these neurons for the development of antiobesity therapies.

The DMH is recognized as a brain center that promotes energy expenditure in part through the activation of thermogenesis in BAT (14, 42). Interestingly, we observed that DMH^{TrkB} neurons can be activated by either warm or cold temperatures. However, statistical analysis revealed that there is no interaction between temperature and location, indicating that there is not a region-specific sensitivity of DMH^{TrkB} neurons to a particular temperature. Furthermore, previous studies have shown that stress can activate separate populations of neurons in the dorsal and central/ventral DMH compartments that project to the RPa and the PVH, respectively (12). Given the extreme temperatures that mice were exposed to during this experiment, it is reasonable to assume that some Fos^{+} DMH^{TrkB} neurons we detected in our experiment are nonspecifically responsive to stress rather than temperature. Thus, we cannot conclude that DMH^{TrkB} neurons can be definitively divided into warm- and cold-sensitive populations.

Neurons located in the anterior and dorsal compartments of the DMH that project to the RPa mediate increased sympathetic tone in BAT, leading to thermogenesis (12, 15, 43). Consistent with these reports, we found that activation of $DMH^{TrkB\rightarrow RPa}$ neurons induces heat production and *Ucp1* expression in BAT. However, $DMH^{TrkB\rightarrow RPa}$ neurons are more broadly distributed than previously characterized DMH→RPa neurons in the dorsal DMH. Although cell body fluorescent signals in $DMH^{TrkB\rightarrow RPa}$:mCherry mice appear concentrated in the dorsal DMH, detection of mCherry expression by ISH reveals numerous $DMH^{TrkB\rightarrow RPa}$ neurons in the central and ventral compartments of the DMH. Additionally, activation of DMH^{TrkB} neurons has no obvious effect on cardiovascular physiology, which is in contrast to other DMH → RPa sympathoexcitatory projections that lead to increased heart rate and blood pressure (12, 15, 16). The specificity of the $DMH^{TrkB\rightarrow RPa}$ neuron function may be reflective of the selectivity of DMH^{TrkB} neurocircuitry, which we see forms connections with BAT, but not the heart; however, it is unclear how autonomic selectivity for peripheral tissues is retained at the level of the RPa.

Previously described populations of RPa-projecting DMH neurons have predominantly been glutamatergic. Our ISH results reveal that $DMH^{TrkB\rightarrow RPa}$ neurons are heterogeneous, comprising almost equally of excitatory and inhibitory populations as well as those that do not appear to express either Vglut2 or Vgat. Inhibitory input to RPa neurons has only been implicated in the negative regulation of thermogenesis and has not been described to increase body temperature (11). Thus, we speculate that subsets of $DMH^{TrkB\rightarrow RPa}$ neurons might target different populations of RPa neurons and act in concert to promote thermogenesis while inhibiting increases in heart rate or blood pressure. Future investigations aimed at characterizing the molecular diversity of DMH^{TrkB} neurons by single-cell RNA sequencing methods to find more specific markers that would distinguish the Vgat, Vglut2, and other populations are necessary. Dissecting the neurocircuitry from the DMH to targets in the RPa will provide useful insight into the mechanisms of functional autonomic selectivity that hold therapeutic value for treating cardiovascular disease.

Food intake represents the positive arm of energy balance, which shares equal importance with energy expenditure for regulating body weight. Our previous studies indicate that TrkB expression in the DMH and DMH^{TrkB} neuron activity are necessary for regulating homeostatic feeding that is dependent on the time of day (21). In this study, we identify the PVH and POA as specific brain regions that are targeted by DMH^{TrkB} neurons to inhibit feeding. Inhibitory input to *Bmal1*-expressing neurons in the PVH has recently been implicated in maintaining normal rhythmicity in feeding and metabolism (44); however, the source of this inhibition is unclear. It is possible that the inhibitory population of $DMH^{TrkB\rightarrow PVH}$ neurons we identified could suppress the activity of PVH^{Bmal1} neurons to maintain normal metabolic and feeding rhythmicity. We also see that many $DMH^{TrkB\rightarrow PVH}$ neurons express the excitatory marker, Vglut2. These glutamatergic $DMH^{TrkB\rightarrow PVH}$ neurons might contribute to the suppression of feeding by acting on established anorexigenic neuron populations in the PVH, including those that express BDNF (38, 45, 46). BDNF signaling through TrkB is critical for neural circuit development and synaptic plasticity (47); thus, PVH^{BDNF} neurons represent an attractive potential neural substrate for $DMH^{TrkB\rightarrow PVH}$ neurons that govern feeding.

Given that activation of $DMH^{TrkB\rightarrow RPa}$ neurons does not drive energy expenditure to the full extent seen by stimulating the global DMH^{TrkB} population, other DMH^{TrkB} neurocircuits likely contribute to increased total energy expenditure. $DMH^{TrkB\rightarrow PVH}$ neurons might help facilitate BAT activity by inhibiting nucleus tractus solitarius (NTS)-projecting PVH neurons that negatively regulate the RPa (48, 49) or by exciting PVH^{BDNF} neurons that are polysynaptically connected to BAT (38). This possibility is in line with the subtle thermogenic effect of activating a DMH^{TrkB} → PVH neurocircuit. Despite significant overlap in retrogradely labeled DMH^{TrkB} populations that project to the PVH and the POA, activation of $DMH^{TrkB\rightarrow POA}$ neurons was not sufficient to significantly increase BAT temperature or energy expenditure as was observed for activation of $DMH^{TrkB\rightarrow PVH}$ neurons. This discrepancy may be due to an incomplete activation of all $DMH^{TrkB\rightarrow POA}$ neurons, attributed to the limited expression of retrograde FLPo-expressing virus at the VMPO. Alternatively, $DMH^{TrkB\rightarrow PVH}$ neurons that drive thermogenesis and energy expenditure could represent a subpopulation that does not send collaterals to the POA. A yet unknown DMH^{TrkB} neurocircuit that promotes physical activity could also contribute to the increase in total energy expenditure observed upon activating DMH^{TrkB} neurons.

Materials and Methods

Mice. The Ai9/+ mouse strain [Gt(ROSA)26Sortm9(CAG-tdTomato)Hze/J; stock number 007909] was acquired from Jackson Laboratory. The *Ntrk2*$^{CreER/+}$ (also known as $TrkB^{CreER}$) mouse strain was generously provided by Dr. David Ginty (Harvard Medical School). Male and female mice aged 6 to 12 wk old were used for initial investigations of chemogenetic activation or inhibition of global DMH^{TrkB} neurons. Both males and females showed similar phenotypes; thus, only female mice were used for subsequent projection specific manipulation of DMH^{TrkB} neuronal activity. Details on animal housing and drug treatments can be found in *SI Appendix, Supplementary Materials and Methods*. All experiments were performed in accordance with relevant guidelines and regulations regarding the use of experimental animals. The Animal Care and Use Committees at The Scripps Research Institute Florida approved all animal procedures used in this study.

Viruses and Plasmid Construction. AAV2-CMV-GFP (4.4×10^{12} vg/mL; The University of North Carolina at Chapel Hill [UNC] Vector Core), AAV2-CAG--FLEX-tdTomato (4.8×10^{12} vg/mL, UNC Vector Core), AAV8-hSyn-DIO-hM3-mCherry (4×10^{12} vg/mL, Addgene 44362), AAV8-hSyn-hM4-mCherry (6×10^{12} vg/mL, UNC Vector Core), and AAV8-hSyn-mCherry (2.1×10^{13} vg/mL, Addgene) were used. AAV2-retro-EF1a-DIO-FLPo (2.6×10^{13} vg/mL) was packaged by Vigene Biosciences from pAAV-EF1a-DIO-FLPo-WPRE-hGHpA (a gift from Li Zhang, Addgene 87306). AAV2-fDIO-mCherry was previously described (41) (4.2×10^{12} vg/mL, packaged by Vigene), and AAV2-fDIO-hM3-mCherry (6.64×10^{12} vg/mL, packaged by Vigene) was similarly constructed; pAAV-hSyn-DIO-hM3-mCherry (a gift from Brian Roth, Addgene 44361) and pAAV-EF1a-f-DIO-EYFP (a gift from Karl Deisseroth, Addgene 55461) were digested with AscI and NheI, and the hM3-mCherry fragment was ligated into pAAV-EF1a-fDIO backbone. The resulting pAAV-EF1a-fDIO-hM3-mCherry plasmid was confirmed by sequencing and additional digestion with XmaI prior to commercial packaging. Herpes simplex virus (HSV)129ΔTK-tdTomato was obtained from the Center for Neuroanatomy with Neurotropic Viruses.

Immunohistochemistry. For Fos staining, mice were perfused with 4% paraformaldehyde (PFA), and the brain was dissected and postfixed overnight in 4% PFA. Brains were cryoprotected, and 40-μm-thick sections were collected with a sliding microtome (Leica) and immunostained before fluorescent imaging and quantification. For analysis of anterograde tracing in BAT and heart tissues, 20-μm frozen sections were collected with a cryostat (Leica). Details are available in *SI Appendix, Supplementary Materials and Methods*.

Stereotaxic Surgery. *Ntrk2*$^{CreER/+}$ mice at 6 to 8 wk of age underwent stereotactic delivery of AAV viruses followed by 1 wk of recovery and 1 wk of tamoxifen treatment. Mice injected with HSV129ΔTK were pretreated with tamoxifen 2 d before viral delivery and continued to be treated on postoperative days 1 through 4. Injection coordinates (anterior-posterior [AP], mediolateral [ML], and dorsoventral [DV]) were as follows: POA (AP, +0.60 mm; ML, ±0.35 mm; and DV, −5.70 mm), PVH (AP, −0.50 mm; ML, ±0.35 mm; and DV, −5.30 mm), DMH (AP, −1.50 mm; ML, ±0.35 mm; and DV, −5.70 mm), and RPa (AP, −6.00 mm; ML, 0.00 mm; and DV, −6.35 mm). Additional information is available in *SI Appendix, Supplementary Materials and Methods*.

Temperature Measurements. Core body temperature was determined with a digital thermometer (Fisher Traceable Type K thermometer) with rodent rectal temperature probe (World Precision Instruments, RET-3).

For thermal imaging experiments, the fur on the back of mice was shaved, and a thermal camera (FLIR E53sc) was mounted above a cage with mice. Thermal images were collected 1 h after injection of vehicle or CNO, and regions above the shoulders (above interscapular BAT), lumbar area (body), and tail were analyzed using ResearchIR software (FLIR). Details are available in *SI Appendix, Supplementary Materials and Methods*.

Physiological Measurements. Locomotor activity and oxygen consumption in individual mice were measured using a Columbus Instruments' Comprehensive Lab Animal Monitoring System. Mice received a vehicle intraperitoneal (i.p.) injection in the morning (between 8 and 9 AM) and a second i.p. injection with CNO (between 12 and 1 PM). Physical activity and metabolic data were collected for 4 h following treatment with either vehicle or CNO. Heart rate and blood pressure were recorded using a tail cuff system (MC4000, Hatteras Instruments), and nocturnal food intake studies were performed as previously described (21). Additional details can be found in *SI Appendix, Supplementary Materials and Methods*.

Quantitative RT-PCR. BAT tissue was dissected 2 h after injection of CNO and snap-frozen in liquid nitrogen prior to extraction of total RNA. Following reverse transcription (New England Biolabs, M0253), qPCR was carried out using SYBR green mix (Roche) in an StepOne cycler (Applied Biosystems). Additional details and primer sequences are available in *SI Appendix, Supplementary Materials and Methods*.

Immunoblotting. Protein was extracted from BAT samples, resolved by sodium dodecyl sulfate-polyacrylamide gel electrophoresis (SDS-PAGE), and transferred to polyvinylidene difluoride membrane. Membranes were blocked in 5% milk and immunoblotted for p-HSL, HSL, and β-actin. Densitometric analysis of bands was performed using ImageJ software. Further details are available in *SI Appendix, Supplementary Materials and Methods*.

Glycerol Measurement. Glycerol content of BAT from mice expressing either mCherry or hM3 in DMH^{TrkB} neurons and treated with CNO (1.5 mg/kg) was determined using a Glycerol-Glo Assay (Promega, J3150) according to the manufacturer's instructions. Details are available in *SI Appendix, Supplementary Materials and Methods*.

In Situ Hybridization. Brains from DMH$^{TrkB\rightarrow RPa}$:mCherry and DMH$^{TrkB\rightarrow PVH}$:mCherry mice were dissected and immediately frozen on dry ice and stored at −80 °C. Prior to sectioning, samples were embedded in optimal cutting temperature compound (OCT) (Tissue Tek). Fresh frozen sections (14 μm) were collected with a cryostat (Leica) onto Superfrost Plus slides (Fisherbrand, 12-550-15). Fluorescent ISH was carried out according to the manufacturer's instructions (ACD, RNAScope Multiplex Fluorescent detection kit v2, 323110). More details are available in *SI Appendix, Supplementary Materials and Methods*.

Statistical Analyses. All data are presented as means ± SEM. Graphs and statistical analyses were generated using GraphPad Prism software. Statistical significance was determined using either two-tailed unpaired Student's *t* test or two-way ANOVA when comparing more than two groups. All experiments were performed at least three times independently or in three separate animals. All statistical analyses are listed in *SI Appendix*, Table S1.

Data Availability. All study data are included in the article and/or *SI Appendix*.

ACKNOWLEDGMENTS. This work was supported by grants from the NIH to B.X. (R01 DK105954 and R01 DK103335) and J.H. (F32 NS106810). HSV129ΔTK-TT was provided by the Center for Neuroanatomy with Neurotropic Viruses, which was supported by an NIH grant (P40 RR018604).

1. A. Hruby, F. B. Hu, The epidemiology of obesity: A big picture. *Pharmacoeconomics* **33**, 673–689 (2015).
2. R. L. Leibel, M. Rosenbaum, J. Hirsch, Changes in energy expenditure resulting from altered body weight. *N. Engl. J. Med.* **332**, 621–628 (1995).
3. K. Lotfi, K. Palmer, C. M. Apovian, Case Study: Weight loss in a patient with type 2 diabetes: Challenges of diabetes management. *Obesity (Silver Spring)* **23** (suppl. 1), S11–S12 (2015).
4. K. Y. Chen *et al*., Opportunities and challenges in the therapeutic activation of human energy expenditure and thermogenesis to manage obesity. *J. Biol. Chem.* **295**, 1926–1942 (2020).
5. G. Z. Kalil, W. G. Haynes, Sympathetic nervous system in obesity-related hypertension: mechanisms and clinical implications. *Hypertens. Res.* **35**, 4–16 (2012).
6. B. B. Lowell, B. M. Spiegelman, Towards a molecular understanding of adaptive thermogenesis. *Nature* **404**, 652–660 (2000).
7. Y. Nakamura *et al*., Direct pyrogenic input from prostaglandin EP3 receptor-expressing preoptic neurons to the dorsomedial hypothalamus. *Eur. J. Neurosci.* **22**, 3137–3146 (2005).
8. C. L. Tan *et al*., Warm-sensitive neurons that control body temperature. *Cell* **167**, 47–59.e15 (2016).
9. Z. D. Zhao *et al*., A hypothalamic circuit that controls body temperature. *Proc. Natl. Acad. Sci. U.S.A.* **114**, 2042–2047 (2017).
10. K. Nakamura *et al*., Identification of sympathetic premotor neurons in medullary raphe regions mediating fever and other thermoregulatory functions. *J. Neurosci.* **24**, 5370–5380 (2004).
11. M. Schneeberger *et al*., Regulation of energy expenditure by brainstem GABA neurons. *Cell* **178**, 672–685.e12 (2019).
12. N. Kataoka, H. Hioki, T. Kaneko, K. Nakamura, Psychological stress activates a dorsomedial hypothalamus-medullary raphe circuit driving brown adipose tissue thermogenesis and hyperthermia. *Cell Metab.* **20**, 346–358 (2014).
13. W. H. Cao, S. F. Morrison, Glutamate receptors in the raphe pallidus mediate brown adipose tissue thermogenesis evoked by activation of dorsomedial hypothalamic neurons. *Neuropharmacology* **51**, 426–437 (2006).
14. M. V. Zaretskaia, D. V. Zaretsky, A. Shekhar, J. A. DiMicco, Chemical stimulation of the dorsomedial hypothalamus evokes non-shivering thermogenesis in anesthetized rats. *Brain Res.* **928**, 113–125 (2002).
15. R. A. Piñol *et al*., Brs3 neurons in the mouse dorsomedial hypothalamus regulate body temperature, energy expenditure, and heart rate, but not food intake. *Nat. Neurosci.* **21**, 1530–1540 (2018).
16. S. E. Simonds *et al*., Leptin mediates the increase in blood pressure associated with obesity. *Cell* **159**, 1404–1416 (2014).
17. L. L. Bellinger, L. L. Bernardis, The dorsomedial hypothalamic nucleus and its role in ingestive behavior and body weight regulation: Lessons learned from lesioning studies. *Physiol. Behav.* **76**, 431–442 (2002).
18. Z. Otgon-Uul, S. Suyama, H. Onodera, T. Yada, Optogenetic activation of leptin- and glucose-regulated GABAergic neurons in dorsomedial hypothalamus promotes food intake via inhibitory synaptic transmission to paraventricular nucleus of hypothalamus. *Mol. Metab.* **5**, 709–715 (2016).
19. A. S. Garfield *et al*., Dynamic GABAergic afferent modulation of AgRP neurons. *Nat. Neurosci.* **19**, 1628–1635 (2016).
20. A. R. Rau, S. T. Hentges, GABAergic inputs to POMC neurons originating from the dorsomedial hypothalamus are regulated by energy state. *J. Neurosci.* **39**, 6449–6459 (2019).
21. G. Y. Liao, C. E. Kinney, J. J. An, B. Xu, TrkB-expressing neurons in the dorsomedial hypothalamus are necessary and sufficient to suppress homeostatic feeding. *Proc. Natl. Acad. Sci. U.S.A.* **116**, 3256–3261 (2019).
22. J. Chen, K. A. Scott, Z. Zhao, T. H. Moran, S. Bi, Characterization of the feeding inhibition and neural activation produced by dorsomedial hypothalamic cholecystokinin administration. *Neuroscience* **152**, 178–188 (2008).
23. T. Sonoyama *et al*., Human BDNF/TrkB variants impair hippocampal synaptogenesis and associate with neurobehavioural abnormalities. *Sci. Rep.* **10**, 9028 (2020).
24. Y. Zhang *et al*., Leptin-receptor-expressing neurons in the dorsomedial hypothalamus and median preoptic area regulate sympathetic brown adipose tissue circuits. *J. Neurosci.* **31**, 1873–1884 (2011).
25. M. Rutlin *et al*., The cellular and molecular basis of direction selectivity of Aδ-LTMRs. *Cell* **159**, 1640–1651 (2014).Corrected in: *Cell* **160**, 1027 (2015).
26. L. Madisen *et al*., A robust and high-throughput Cre reporting and characterization system for the whole mouse brain. *Nat. Neurosci.* **13**, 133–140 (2010).
27. M. E. Greenberg, E. B. Ziff, L. A. Greene, Stimulation of neuronal acetylcholine receptors induces rapid gene transcription. *Science* **234**, 80–83 (1986).

28. G. M. Alexander *et al*., Remote control of neuronal activity in transgenic mice expressing evolved G protein-coupled receptors. *Neuron* **63**, 27–39 (2009).
29. A. W. Fischer, B. Cannon, J. Nedergaard, Optimal housing temperatures for mice to mimic the thermal environment of humans: An experimental study. *Mol. Metab.* **7**, 161-170 (2017).
30. C. W. Meyer, Y. Ootsuka, A. A. Romanovsky, Body temperature measurements for metabolic phenotyping in mice. *Front. Physiol.* **8**, 520 (2017).
31. J. L. Gomez *et al*., Chemogenetics revealed: DREADD occupancy and activation via converted clozapine. *Science* **357**, 503–507 (2017).
32. H. S. Vestri, L. Maianu, D. R. Moellering, W. T. Garvey, Atypical antipsychotic drugs directly impair insulin action in adipocytes: Effects on glucose transport, lipogenesis, and antilipolysis. *Neuropsychopharmacology* **32**, 765–772 (2007).
33. W. W. Blessing, A. Zilm, Y. Ootsuka, Clozapine reverses increased brown adipose tissue thermogenesis induced by 3,4-methylenedioxymethamphetamine and by cold exposure in conscious rats. *Neuroscience* **141**, 2067–2073 (2006).
34. T. M. Takahashi *et al*., A discrete neuronal circuit induces a hibernation-like state in rodents. *Nature* **583**, 109–114 (2020).
35. N. A. Brito, M. N. Brito, T. J. Bartness, Differential sympathetic drive to adipose tissues after food deprivation, cold exposure or glucoprivation. *Am. J. Physiol. Regul. Integr. Comp. Physiol.* **294**, R1445–R1452 (2008).
36. D. Tupone, C. J. Madden, S. F. Morrison, Autonomic regulation of brown adipose tissue thermogenesis in health and disease: Potential clinical applications for altering BAT thermogenesis. *Front. Neurosci.* **8**, 14 (2014).
37. K. Rezai-Zadeh *et al*., Leptin receptor neurons in the dorsomedial hypothalamus are key regulators of energy expenditure and body weight, but not food intake. *Mol. Metab.* **3**, 681–693 (2014).
38. J. J. An, G. Y. Liao, C. E. Kinney, N. Sahibzada, B. Xu, Discrete BDNF neurons in the paraventricular hypothalamus control feeding and energy expenditure. *Cell Metab.* **22**, 175–188 (2015).
39. G. S. Yeo *et al*., A de novo mutation affecting human TrkB associated with severe obesity and developmental delay. *Nat. Neurosci.* **7**, 1187–1189 (2004).
40. B. Xu *et al*., Brain-derived neurotrophic factor regulates energy balance downstream of melanocortin-4 receptor. *Nat. Neurosci.* **6**, 736–742 (2003).
41. J. J. An *et al*., TrkB-expressing paraventricular hypothalamic neurons suppress appetite through multiple neurocircuits. *Nat. Commun.* **11**, 1729 (2020).
42. N. Zhang, L. Yang, L. Guo, S. Bi, Activation of dorsomedial hypothalamic neurons promotes physical activity and decreases food intake and body weight in zucker fatty rats. *Front. Mol. Neurosci.* **11**, 179 (2018).
43. S. Yu *et al*., Glutamatergic preoptic area neurons that express leptin receptors drive temperature-dependent body weight homeostasis. *J. Neurosci.* **36**, 5034–5046 (2016).
44. E. R. Kim *et al*., Paraventricular hypothalamus mediates diurnal rhythm of metabolism. *Nat. Commun.* **11**, 3794 (2020).
45. M. M. Li *et al*., The paraventricular hypothalamus regulates satiety and prevents obesity via two genetically distinct circuits. *Neuron* **102**, 653–667.e6 (2019).
46. Y. Xu *et al*., Glutamate mediates the function of melanocortin receptor 4 on Sim1 neurons in body weight regulation. *Cell Metab.* **18**, 860–870 (2013).
47. E. J. Huang, L. F. Reichardt, Neurotrophins: Roles in neuronal development and function. *Annu. Rev. Neurosci.* **24**, 677–736 (2001).
48. D. Kong *et al*., GABAergic RIP-Cre neurons in the arcuate nucleus selectively regulate energy expenditure. *Cell* **151**, 645–657 (2012).
49. C. J. Madden, S. F. Morrison, Neurons in the paraventricular nucleus of the hypothalamus inhibit sympathetic outflow to brown adipose tissue. *Am. J. Physiol. Regul. Integr. Comp. Physiol.* **296**, R831–R843 (2009).